

Search for a massless dark photon in $\Lambda_c^+ \rightarrow p\gamma'$ decay

- M. Ablikim¹, M. N. Achasov^{11,b}, P. Adlarson⁷⁰, M. Albrecht⁴, R. Aliberti³¹, A. Amoroso^{69A,69C}, M. R. An³⁵, Q. An^{66,53}, X. H. Bai⁶¹, Y. Bai⁵², O. Bakina³², R. Baldini Ferroli^{26A}, I. Balossino^{27A}, Y. Ban^{42,g}, V. Batozskaya^{1,40}, D. Becker³¹, K. Begzsuren²⁹, N. Berger³¹, M. Bertani^{26A}, D. Bettone^{27A}, F. Bianchi^{69A,69C}, J. Bloms⁶³, A. Bortone^{69A,69C}, I. Boyko³², R. A. Briere⁵, A. Brueggemann⁶³, H. Cai⁷¹, X. Cai^{1,53}, A. Calcaterra^{26A}, G. F. Cao^{1,58}, N. Cao^{1,58}, S. A. Cetin^{57A}, J. F. Chang^{1,53}, W. L. Chang^{1,58}, G. Chelkov^{32,a}, C. Chen³⁹, Chao Chen⁵⁰, G. Chen¹, H. S. Chen^{1,58}, M. L. Chen^{1,53}, S. J. Chen³⁸, S. M. Chen⁵⁶, T. Chen¹, X. R. Chen^{28,58}, X. T. Chen¹, Y. B. Chen^{1,53}, Z. J. Chen^{23,h}, W. S. Cheng^{69C}, S. K. Choi⁵⁰, X. Chu³⁹, G. Cibinetto^{27A}, F. Cossio^{69C}, J. J. Cui⁴⁵, H. L. Dai^{1,53}, J. P. Dai⁷³, A. Dbeysi¹⁷, R. E. de Boer⁴, D. Dedovich³², Z. Y. Deng¹, A. Denig³¹, I. Denysenko³², M. Destefanis^{69A,69C}, F. De Mori^{69A,69C}, Y. Ding³⁶, J. Dong^{1,53}, L. Y. Dong^{1,58}, M. Y. Dong^{1,53,58}, X. Dong⁷¹, S. X. Du⁷⁵, P. Egorov^{32,a}, Y. L. Fan⁷¹, J. Fang^{1,53}, S. S. Fang^{1,58}, W. X. Fang¹, Y. Fang¹, R. Farinelli^{27A}, L. Fava^{69B,69C}, F. Feldbauer⁴, G. Felici^{26A}, C. Q. Feng^{66,53}, J. H. Feng⁵⁴, K. Fischer⁶⁴, M. Fritsch⁴, C. Fritzsch⁶³, C. D. Fu¹, H. Gao⁵⁸, Y. N. Gao^{42,g}, Yang Gao^{66,53}, S. Garbolino^{69C}, I. Garzia^{27A,27B}, P. T. Ge⁷¹, Z. W. Ge³⁸, C. Geng⁵⁴, E. M. Gersabeck⁶², A. Gilman⁶⁴, K. Goetzen¹², L. Gong³⁶, W. X. Gong^{1,53}, W. Gradl³¹, M. Greco^{69A,69C}, L. M. Gu³⁸, M. H. Gu^{1,53}, Y. T. Gu¹⁴, C. Y. Guan^{1,58}, A. Q. Guo^{28,58}, L. B. Guo³⁷, R. P. Guo⁴⁴, Y. P. Guo^{10,f}, A. Guskov^{32,a}, T. T. Han⁴⁵, W. Y. Han³⁵, X. Q. Hao¹⁸, F. A. Harris⁶⁰, K. K. He⁵⁰, K. L. He^{1,58}, F. H. Heinsius⁴, C. H. Heinz³¹, Y. K. Heng^{1,53,58}, C. Herold⁵⁵, M. Himmelreich^{12,d}, M. Himmelreich^{31,d}, G. Y. Hou^{1,58}, Y. R. Hou⁵⁸, Z. L. Hou¹, H. M. Hu^{1,58}, J. F. Hu^{51,i}, T. Hu^{1,53,58}, Y. Hu¹, G. S. Huang^{66,53}, K. X. Huang⁵⁴, L. Q. Huang⁶⁷, L. Q. Huang^{28,58}, X. T. Huang⁴⁵, Y. P. Huang¹, Z. Huang^{42,g}, T. Hussain⁶⁸, N. Hüsken^{25,31}, W. Imoehl²⁵, M. Irshad^{66,53}, J. Jackson²⁵, S. Jaeger⁴, S. Janchiv²⁹, E. Jang⁵⁰, J. H. Jeong⁵⁰, Q. Ji¹, Q. P. Ji¹⁸, X. B. Ji^{1,53}, Y. Y. Ji⁴⁵, Z. K. Jia^{66,53}, H. B. Jiang⁴⁵, S. S. Jiang³⁵, X. S. Jiang^{1,53,58}, Y. Jiang⁵⁸, J. B. Jiao⁴⁵, Z. Jiao²¹, S. Jin³⁸, Y. Jin⁶¹, M. Q. Jing^{1,58}, T. Johansson⁷⁰, N. Kalantar-Nayestanaki⁵⁹, X. S. Kang³⁶, R. Kappert⁵⁹, B. C. Ke⁷⁵, I. K. Keshk⁴, A. Khoukaz⁶³, R. Kiuchi¹, R. Kliment¹², L. Koch³³, O. B. Kolcu^{57A}, B. Kopf⁴, M. Kuemmel⁴, M. Kuessner⁴, A. Kupsc^{40,70}, W. Kühn³³, J. J. Lane⁶², J. S. Lange³³, P. Larin¹⁷, A. Lavania²⁴, L. Lavezzi^{69A,69C}, Z. H. Lei^{66,53}, H. Leithoff³¹, M. Lellmann³¹, T. Lenz³¹, C. Li⁴³, C. Li³⁹, C. H. Li³⁵, Cheng Li^{66,53}, D. M. Li⁷⁵, F. Li^{1,53}, G. Li¹, H. Li⁴⁷, H. Li^{66,53}, H. B. Li^{1,58}, H. J. Li¹⁸, H. N. Li^{51,i}, J. Q. Li⁴, J. S. Li⁵⁴, J. W. Li⁴⁵, Ke Li¹, L. J. Li¹, L. K. Li¹, Lei Li³, M. H. Li³⁹, P. R. Li^{34,j,k}, S. X. Li¹⁰, S. Y. Li⁵⁶, T. Li⁴⁵, W. D. Li^{1,58}, W. G. Li¹, X. H. Li^{66,53}, X. L. Li^{1,58}, Xiaoyu Li^{1,58}, Z. X. Li¹⁴, H. Liang³⁰, H. Liang^{1,58}, H. Liang^{66,53}, Y. F. Liang⁴⁹, Y. T. Liang^{28,58}, G. R. Liao¹³, L. Z. Liao⁴⁵, J. Libby²⁴, A. Limphirat⁵⁵, C. X. Lin⁵⁴, D. X. Lin^{28,58}, T. Lin¹, B. J. Liu¹, C. X. Liu¹, D. Liu^{17,66}, F. H. Liu⁴⁸, Fang Liu¹, Feng Liu⁶, G. M. Liu^{51,i}, H. Liu^{34,j,k}, H. B. Liu¹⁴, H. M. Liu^{1,58}, Huanhuan Liu¹, Huihui Liu¹⁹, J. B. Liu^{66,53}, J. L. Liu⁶⁷, J. Y. Liu^{1,58}, K. Liu¹, K. Y. Liu³⁶, Ke Liu²⁰, L. Liu^{66,53}, Lu Liu³⁹, M. H. Liu^{10,f}, P. L. Liu¹, Q. Liu⁵⁸, S. B. Liu^{66,53}, T. Liu^{10,f}, W. K. Liu³⁹, W. M. Liu^{66,53}, X. Liu^{34,j,k}, Y. Liu^{34,j,k}, Z. A. Liu^{1,53,58}, Z. Q. Liu⁴⁵, X. C. Lou^{1,53,58}, F. X. Lu⁵⁴, H. J. Lu²¹, J. G. Lu^{1,53}, X. L. Lu¹, Y. Lu⁷, Y. P. Lu^{1,53}, Z. H. Lu¹, C. L. Luo³⁷, M. X. Luo⁷⁴, T. Luo^{10,f}, X. L. Luo^{1,53}, X. R. Lyu⁵⁸, Y. F. Lyu³⁹, F. C. Ma³⁶, H. L. Ma¹, L. L. Ma⁴⁵, M. M. Ma^{1,58}, Q. M. Ma¹, R. Q. Ma^{1,58}, R. T. Ma⁵⁸, X. Y. Ma^{1,53}, Y. Ma^{42,g}, F. E. Maas¹⁷, M. Maggiora^{69A,69C}, S. Maldaner⁴, S. Malde⁶⁴, Q. A. Malik⁶⁸, A. Mangoni^{26B}, Y. J. Mao^{42,g}, Z. P. Mao¹, S. Marcello^{69A,69C}, Z. X. Meng⁶¹, G. Mezzadri^{27A}, H. Miao¹, T. J. Min³⁸, R. E. Mitchell²⁵, X. H. Mo^{1,53,58}, N. Yu. Muchnoi^{11,b}, Y. Nefedov³², F. Nerling^{17,d}, I. B. Nikolaev^{11,b}, Z. Ning^{1,53}, S. Nisar^{9,l}, Y. Niu⁴⁵, S. L. Olsen⁵⁸, Q. Ouyang^{1,53,58}, S. Pacetti^{26B,26C}, X. Pan^{10,f}, Y. Pan⁵², A. Pathak³⁰, M. Pelizaeus⁴, H. P. Peng^{66,53}, K. Peters^{12,d}, J. L. Ping³⁷, R. G. Ping^{1,58}, S. Plura³¹, S. Pogodin³², F. Z. Qi¹, H. Qi^{66,53}, H. R. Qi⁵⁶, M. Qi³⁸, T. Y. Qi^{10,f}, S. Qian^{1,53}, W. B. Qian⁵⁸, Z. Qian⁵⁴, C. F. Qiao⁵⁸, J. J. Qin⁶⁷, L. Q. Qin¹³, X. P. Qin^{10,f}, X. S. Qin⁴⁵, Z. H. Qin^{1,53}, J. F. Qiu¹, S. Q. Qu⁵⁶, K. H. Rashid⁶⁸, C. F. Redmer³¹, K. J. Ren³⁵, A. Rivetti^{69C}, V. Rodin⁵⁹, M. Rolo^{69C}, G. Rong^{1,58}, Ch. Rosner¹⁷, S. N. Ruan³⁹, H. S. Sang⁶⁶, A. Sarantsev^{32,c}, Y. Schelhaas³¹, C. Schnier⁴, K. Schoenning⁷⁰, M. Scodeggio^{27A,27B}, K. Y. Shan^{10,f}, W. Shan²², X. Y. Shan^{66,53}, J. F. Shangguan⁵⁰, L. G. Shao^{1,58}, M. Shao^{66,53}, C. P. Shen^{10,f}, H. F. Shen^{1,58}, X. Y. Shen^{1,58}, B. A. Shi⁵⁸, H. C. Shi^{66,53}, J. Y. Shi¹, q. q. Shi⁵⁰, R. S. Shi^{1,58}, X. Shi^{1,53}, X. D. Shi^{66,53}, J. J. Song¹⁸, W. M. Song^{30,1}, Y. X. Song^{42,g}, S. Sosio^{69A,69C}, S. Spataro^{69A,69C}, F. Stieler³¹, K. X. Su⁷¹, P. P. Su⁵⁰, Y. J. Su⁵⁸, G. X. Sun¹, H. Sun⁵⁸, H. K. Sun¹, J. F. Sun¹⁸, L. Sun⁷¹, S. S. Sun^{1,58}, T. Sun^{1,58}, W. Y. Sun³⁰, X. Sun^{23,h}, Y. J. Sun^{66,53}, Y. Z. Sun¹, Z. T. Sun⁴⁵, Y. H. Tan⁷¹, Y. X. Tan^{66,53}, C. J. Tang⁴⁹, G. Y. Tang¹, J. Tang⁵⁴, L. Y. Tao⁶⁷, Q. T. Tao^{23,h}, M. Tat⁶⁴, J. X. Teng^{66,53}, V. Thoren⁷⁰, W. H. Tian⁴⁷, Y. Tian^{28,58}, I. Uman^{57B}, B. Wang¹, B. L. Wang⁵⁸, C. W. Wang³⁸, D. Y. Wang^{42,g}, F. Wang⁶⁷, H. J. Wang^{34,j,k}, H. P. Wang^{1,58}, K. Wang^{1,53}, L. L. Wang¹, M. Wang⁴⁵, M. Z. Wang^{42,g}, Meng Wang^{1,58}, S. Wang¹³, S. Wang^{10,f}, T. Wang^{10,f}, T. J. Wang³⁹, W. Wang⁵⁴, W. H. Wang⁷¹, W. P. Wang^{66,53}, X. Wang^{42,g}, X. F. Wang^{34,j,k}, X. L. Wang^{10,f}, Y. Wang⁵⁶, Y. D. Wang⁴¹, Y. F. Wang^{1,53,58}, Y. H. Wang⁴³, Y. Q. Wang¹, Yaqian Wang^{16,1}, Z. Wang^{1,53}, Z. Y. Wang^{1,58}, Ziyi Wang⁵⁸, D. H. Wei¹³, F. Weidner⁶³, S. P. Wen¹, D. J. White⁶², U. Wiedner⁴, G. Wilkinson⁶⁴, M. Wolke⁷⁰, L. Wollenberg⁴, J. F. Wu^{1,58}, L. H. Wu¹, L. J. Wu^{1,58}, X. Wu^{10,f}, X. H. Wu³⁰, Y. Wu⁶⁶, Z. Wu^{1,53}, L. Xia^{66,53}, T. Xiang^{42,g}, D. Xiao^{34,j,k}, G. Y. Xiao³⁸, H. Xiao^{10,f}, S. Y. Xiao¹, Y. L. Xiao^{10,f}, Z. J. Xiao³⁷, C. Xie³⁸, X. H. Xie^{42,g}, Y. Xie⁴⁵, Y. G. Xie^{1,53}, Y. H. Xie⁶, Z. P. Xie^{66,53}, T. Y. Xing^{1,58}, C. F. Xu¹, C. J. Xu⁵⁴, G. F. Xu¹, H. Y. Xu⁶¹, Q. J. Xu¹⁵, X. P. Xu⁵⁰, Y. C. Xu⁵⁸, Z. P. Xu³⁸, F. Yan^{10,f}, L. Yan^{10,f}, W. B. Yan^{66,53}, W. C. Yan⁷⁵, H. J. Yang^{46,e}, H. L. Yang³⁰, H. X. Yang¹, L. Yang⁴⁷, S. L. Yang⁵⁸, Tao Yang¹, Y. F. Yang³⁹, Y. X. Yang^{1,58}, Yifan Yang^{1,58}, M. H. Ye⁸, J. H. Yin¹, Z. Y. You⁵⁴, B. X. Yu^{1,53,58}, C. X. Yu³⁹, G. Yu^{1,58}, T. Yu⁶⁷, X. D. Yu^{42,g}, C. Z. Yuan^{1,58}, L. Yuan², S. C. Yuan¹, X. Q. Yuan¹, Y. Yuan^{1,58}, Z. Y. Yuan⁵⁴, C. X. Yue³⁵, A. A. Zafar⁶⁸, F. R. Zeng⁴⁵, X. Zeng⁶, Y. Zeng^{23,h}, Y. H. Zhan⁵⁴, A. Q. Zhang¹, B. L. Zhang¹, B. X. Zhang¹, D. H. Zhang³⁹, G. Y. Zhang¹⁸, H. Zhang⁶⁶, H. H. Zhang⁵⁴, H. H. Zhang³⁰, H. Y. Zhang^{1,53}, J. L. Zhang⁷², J. Q. Zhang³⁷, J. W. Zhang^{1,53,58}, J. X. Zhang^{34,j,k}, J. Y. Zhang¹, J. Z. Zhang^{1,58}, Jianyu Zhang^{1,58}, Jiawei Zhang^{1,58}, L. M. Zhang⁵⁶, L. Q. Zhang⁵⁴, Lei Zhang³⁸, P. Zhang¹, Q. Y. Zhang^{35,75}, Shuihan Zhang^{1,58}, Shulei Zhang^{23,h}, X. D. Zhang⁴¹,

X. M. Zhang¹, X. Y. Zhang⁵⁰, X. Y. Zhang⁴⁵, Y. Zhang⁶⁴, Y. T. Zhang⁷⁵, Y. H. Zhang^{1,53}, Yan Zhang^{66,53}, Yao Zhang¹, Z. H. Zhang¹, Z. Y. Zhang³⁹, Z. Y. Zhang⁷¹, G. Zhao¹, J. Zhao³⁵, J. Y. Zhao^{1,58}, J. Z. Zhao^{1,53}, Lei Zhao^{66,53}, Ling Zhao¹, M. G. Zhao³⁹, Q. Zhao¹, S. J. Zhao⁷⁵, Y. B. Zhao^{1,53}, Y. X. Zhao^{28,58}, Z. G. Zhao^{66,53}, A. Zhemchugov^{32,a}, B. Zheng⁶⁷, J. P. Zheng^{1,53}, Y. H. Zheng⁵⁸, B. Zhong³⁷, C. Zhong⁶⁷, X. Zhong⁵⁴, H. Zhou⁴⁵, L. P. Zhou^{1,58}, X. Zhou⁷¹, X. K. Zhou⁵⁸, X. R. Zhou^{66,53}, X. Y. Zhou³⁵, Y. Z. Zhou^{10,f}, J. Zhu³⁹, K. Zhu¹, K. J. Zhu^{1,53,58}, L. X. Zhu⁵⁸, S. H. Zhu⁶⁵, S. Q. Zhu³⁸, T. J. Zhu⁷², W. J. Zhu^{10,f}, Y. C. Zhu^{66,53}, Z. A. Zhu^{1,58}, B. S. Zou¹, J. H. Zou¹

(BESIII Collaboration)

¹ Institute of High Energy Physics, Beijing 100049, People's Republic of China

² Beihang University, Beijing 100191, People's Republic of China

³ Beijing Institute of Petrochemical Technology, Beijing 102617, People's Republic of China

⁴ Bochum Ruhr-University, D-44780 Bochum, Germany

⁵ Carnegie Mellon University, Pittsburgh, Pennsylvania 15213, USA

⁶ Central China Normal University, Wuhan 430079, People's Republic of China

⁷ Central South University, Changsha 410083, People's Republic of China

⁸ China Center of Advanced Science and Technology, Beijing 100190, People's Republic of China

⁹ COMSATS University Islamabad, Lahore Campus, Defence Road, Off Raiwind Road, 54000 Lahore, Pakistan

¹⁰ Fudan University, Shanghai 200433, People's Republic of China

¹¹ G.I. Budker Institute of Nuclear Physics SB RAS (BINP), Novosibirsk 630090, Russia

¹² GSI Helmholtzcentre for Heavy Ion Research GmbH, D-64291 Darmstadt, Germany

¹³ Guangxi Normal University, Guilin 541004, People's Republic of China

¹⁴ Guangxi University, Nanning 530004, People's Republic of China

¹⁵ Hangzhou Normal University, Hangzhou 310036, People's Republic of China

¹⁶ Hebei University, Baoding 071002, People's Republic of China

¹⁷ Helmholtz Institute Mainz, Staudinger Weg 18, D-55099 Mainz, Germany

¹⁸ Henan Normal University, Xinxiang 453007, People's Republic of China

¹⁹ Henan University of Science and Technology, Luoyang 471003, People's Republic of China

²⁰ Henan University of Technology, Zhengzhou 450001, People's Republic of China

²¹ Huangshan College, Huangshan 245000, People's Republic of China

²² Hunan Normal University, Changsha 410081, People's Republic of China

²³ Hunan University, Changsha 410082, People's Republic of China

²⁴ Indian Institute of Technology Madras, Chennai 600036, India

²⁵ Indiana University, Bloomington, Indiana 47405, USA

²⁶ INFN Laboratori Nazionali di Frascati , (A)INFN Laboratori Nazionali di Frascati, I-00044, Frascati, Italy; (B)INFN Sezione di Perugia, I-06100, Perugia, Italy; (C)University of Perugia, I-06100, Perugia, Italy

²⁷ INFN Sezione di Ferrara, (A)INFN Sezione di Ferrara, I-44122, Ferrara, Italy; (B)University of Ferrara, I-44122, Ferrara, Italy

²⁸ Institute of Modern Physics, Lanzhou 730000, People's Republic of China

²⁹ Institute of Physics and Technology, Peace Avenue 54B, Ulaanbaatar 13330, Mongolia

³⁰ Jilin University, Changchun 130012, People's Republic of China

³¹ Johannes Gutenberg University of Mainz, Johann-Joachim-Becher-Weg 45, D-55099 Mainz, Germany

³² Joint Institute for Nuclear Research, 141980 Dubna, Moscow region, Russia

³³ Justus-Liebig-Universitaet Giessen, II. Physikalisches Institut, Heinrich-Buff-Ring 16, D-35392 Giessen, Germany

³⁴ Lanzhou University, Lanzhou 730000, People's Republic of China

³⁵ Liaoning Normal University, Dalian 116029, People's Republic of China

³⁶ Liaoning University, Shenyang 110036, People's Republic of China

³⁷ Nanjing Normal University, Nanjing 210023, People's Republic of China

³⁸ Nanjing University, Nanjing 210093, People's Republic of China

³⁹ Nankai University, Tianjin 300071, People's Republic of China

⁴⁰ National Centre for Nuclear Research, Warsaw 02-093, Poland

⁴¹ North China Electric Power University, Beijing 102206, People's Republic of China

⁴² Peking University, Beijing 100871, People's Republic of China

⁴³ Qufu Normal University, Qufu 273165, People's Republic of China

⁴⁴ Shandong Normal University, Jinan 250014, People's Republic of China

⁴⁵ Shandong University, Jinan 250100, People's Republic of China

⁴⁶ Shanghai Jiao Tong University, Shanghai 200240, People's Republic of China

⁴⁷ Shanxi Normal University, Linfen 041004, People's Republic of China

⁴⁸ Shanxi University, Taiyuan 030006, People's Republic of China

⁴⁹ Sichuan University, Chengdu 610064, People's Republic of China

⁵⁰ Soochow University, Suzhou 215006, People's Republic of China

⁵¹ South China Normal University, Guangzhou 510006, People's Republic of China

⁵² Southeast University, Nanjing 211100, People's Republic of China

⁵³ State Key Laboratory of Particle Detection and Electronics, Beijing 100049, Hefei 230026, People's Republic of China

- ⁵⁴ Sun Yat-Sen University, Guangzhou 510275, People's Republic of China
⁵⁵ Suranaree University of Technology, University Avenue 111, Nakhon Ratchasima 30000, Thailand
⁵⁶ Tsinghua University, Beijing 100084, People's Republic of China
⁵⁷ Turkish Accelerator Center Particle Factory Group, (A)Istinye University, 34010, Istanbul, Turkey; (B)Near East University, Nicosia, North Cyprus, Mersin 10, Turkey
⁵⁸ University of Chinese Academy of Sciences, Beijing 100049, People's Republic of China
⁵⁹ University of Groningen, NL-9747 AA Groningen, The Netherlands
⁶⁰ University of Hawaii, Honolulu, Hawaii 96822, USA
⁶¹ University of Jinan, Jinan 250022, People's Republic of China
⁶² University of Manchester, Oxford Road, Manchester, M13 9PL, United Kingdom
⁶³ University of Muenster, Wilhelm-Klemm-Strasse 9, 48149 Muenster, Germany
⁶⁴ University of Oxford, Keble Road, Oxford OX13RH, United Kingdom
⁶⁵ University of Science and Technology Liaoning, Anshan 114051, People's Republic of China
⁶⁶ University of Science and Technology of China, Hefei 230026, People's Republic of China
⁶⁷ University of South China, Hengyang 421001, People's Republic of China
⁶⁸ University of the Punjab, Lahore-54590, Pakistan
⁶⁹ University of Turin and INFN, (A)University of Turin, I-10125, Turin, Italy; (B)University of Eastern Piedmont, I-15121, Alessandria, Italy; (C)INFN, I-10125, Turin, Italy
⁷⁰ Uppsala University, Box 516, SE-75120 Uppsala, Sweden
⁷¹ Wuhan University, Wuhan 430072, People's Republic of China
⁷² Xinyang Normal University, Xinyang 464000, People's Republic of China
⁷³ Yunnan University, Kunming 650500, People's Republic of China
⁷⁴ Zhejiang University, Hangzhou 310027, People's Republic of China
⁷⁵ Zhengzhou University, Zhengzhou 450001, People's Republic of China
- ^a Also at the Moscow Institute of Physics and Technology, Moscow 141700, Russia
^b Also at the Novosibirsk State University, Novosibirsk, 630090, Russia
^c Also at the NRC "Kurchatov Institute", PNPI, 188300, Gatchina, Russia
^d Also at Goethe University Frankfurt, 60323 Frankfurt am Main, Germany
^e Also at Key Laboratory for Particle Physics, Astrophysics and Cosmology, Ministry of Education; Shanghai Key Laboratory for Particle Physics and Cosmology; Institute of Nuclear and Particle Physics, Shanghai 200240, People's Republic of China
^f Also at Key Laboratory of Nuclear Physics and Ion-beam Application (MOE) and Institute of Modern Physics, Fudan University, Shanghai 200443, People's Republic of China
^g Also at State Key Laboratory of Nuclear Physics and Technology, Peking University, Beijing 100871, People's Republic of China
^h Also at School of Physics and Electronics, Hunan University, Changsha 410082, China
ⁱ Also at Guangdong Provincial Key Laboratory of Nuclear Science, Institute of Quantum Matter, South China Normal University, Guangzhou 510006, China
^j Also at Frontiers Science Center for Rare Isotopes, Lanzhou University, Lanzhou 730000, People's Republic of China
^k Also at Lanzhou Center for Theoretical Physics, Lanzhou University, Lanzhou 730000, People's Republic of China
^l Also at the Department of Mathematical Sciences, IBA, Karachi , Pakistan

A search for a massless dark photon γ' is conducted using 4.5 fb^{-1} of e^+e^- collision data collected at center-of-mass energies between 4.600 and 4.699 GeV with the BESIII detector at BEPCII. No significant signal is observed, and the upper limit on the branching fraction $\mathcal{B}(\Lambda_c^+ \rightarrow p\gamma')$ is determined to be 8.0×10^{-5} at 90% confidence level.

I. INTRODUCTION

The flavor changing neutral current (FCNC) transitions of the charmed baryon Λ_c^+ are of great interest since they can provide indications for physics beyond the Standard Model (SM). In the framework of the SM, FCNC transitions are strongly suppressed by the Glashow, Iliopoulos and Maiani (GIM) mechanism [1] in the charm sector. The SM predictions for the branching fractions (BFs) of FCNC decays in the charm sector are less than 10^{-9} [2]. The minimal super-symmetric SM with R-parity violation [3] and the two-Higgs-doublet model [4] predict the BFs of the same FCNC decays to be two

to three orders of magnitude larger. Observation of a FCNC decay with the current experimental sensitivity would imply new physics beyond the SM.

Models of new physics beyond the SM may have a dark sector containing an extra Abelian gauge group, $U(1)_D$, under which all the SM fields are singlets. This symmetry may be broken spontaneously or may remain unbroken, causing the associated gauge boson, the dark photon, to acquire a mass or remain massless. These possibilities have received a great deal of attention in recent decades [5–15]. If $U(1)_D$ remains unbroken, there is always a linear combination of the dark and SM Abelian gauge fields which does not have renormalizable cou-

plings to SM members and which can be identified with the massless dark photon (γ') [5, 6]. While it has no direct interactions with SM fermions, the γ' can still exert influence on the SM via higher-dimensional operators generated by loop diagrams involving particles that are charged under $U(1)_D$ and also coupled to SM fields [6–8].

In experiment, LHCb reported the evidence for the breaking of lepton universality in bottom-quark FCNC decays to charged lepton pairs with a significance of 3.1σ [16]. As a complementary study, we concentrate on FCNC effects arising from the dark photon with the c and u quarks, where the missing energy due to the dark photon is the feature of the signal processes. BESIII has searched for the invisible signals within various hadron decays, including $\eta/\eta' \rightarrow$ invisible [17], $\omega/\phi \rightarrow$ invisible [18], $\Lambda \rightarrow$ invisible [19] and $J/\psi \rightarrow \gamma +$ invisible [20], and no significant signals are observed. However, this has never been probed in the charmed baryon sector. The two-body charmed baryon decay potentially offers a competitive window to access $c \rightarrow u\gamma'$, which gives rise to the FCNC decays of charmed baryon into a lighter baryon plus missing energy carried away by the massless dark photon. Figure 1 presents a typical Feynman diagram of $\Lambda_c^+ \rightarrow p\gamma'$. It is found that the BFs of some charmed baryon decays are allowed to be as high as a few times 10^{-5} [21]. Such BFs are likely to be within the sensitivity reaches of some ongoing experiments like BESIII.

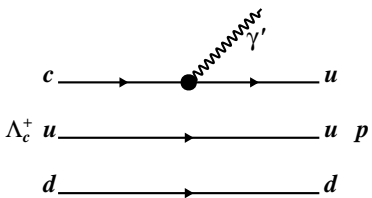


Fig. 1: Feynman diagram for $\Lambda_c^+ \rightarrow p\gamma'$.

This paper presents an experimental search for a massless dark photon in $\Lambda_c^+ \rightarrow p\gamma'$ decay using 4.5 fb^{-1} of e^+e^- collision data collected with the BESIII detector at seven center-of-mass (CM) energies between 4.600 and 4.699 GeV. The CM energies and the integrated luminosities for each energy point are listed in Table 1 [26–28]. Taking advantage of the $\Lambda_c^+\bar{\Lambda}_c^-$ production just above the mass threshold 4572.92 MeV, a double-tag (DT) approach [22] is implemented. Throughout the text, the charge conjugate states are always implied.

II. BESIII DETECTOR AND MONTE CARLO SIMULATION

The BESIII detector [23] records symmetric e^+e^- collisions provided by the BEPCII storage ring, which operates with a peak luminosity of $1 \times 10^{33} \text{ cm}^{-2}\text{s}^{-1}$ in the

Table 1: The CM energies and the integrated luminosities (\mathcal{L}_{int}) for each energy point. The first and the second uncertainties are statistical and systematic, respectively.

\sqrt{s} (MeV)	\mathcal{L}_{int} (pb^{-1})
$4599.53 \pm 0.07 \pm 0.74$	$586.90 \pm 0.10 \pm 3.90$
$4611.86 \pm 0.12 \pm 0.32$	$103.83 \pm 0.05 \pm 0.55$
$4628.00 \pm 0.06 \pm 0.32$	$521.52 \pm 0.11 \pm 2.76$
$4640.91 \pm 0.06 \pm 0.38$	$552.41 \pm 0.12 \pm 2.93$
$4661.24 \pm 0.06 \pm 0.29$	$529.63 \pm 0.12 \pm 2.81$
$4681.92 \pm 0.08 \pm 0.29$	$1669.31 \pm 0.21 \pm 8.85$
$4698.82 \pm 0.10 \pm 0.39$	$536.45 \pm 0.12 \pm 2.84$

CM energy range from 2.0 GeV to 4.9 GeV. BESIII has collected large data samples at these energy regions [24]. The cylindrical core of the BESIII detector covers 93% of the full solid angle and consists of a helium-based multilayer drift chamber (MDC), a plastic scintillator time-of-flight system (TOF), and a CsI(Tl) electromagnetic calorimeter (EMC), which are all enclosed in a superconducting solenoidal magnet providing a 1.0 T magnetic field. The solenoid is supported by an octagonal flux-return yoke with resistive plate counter based muon identification modules interleaved with steel. The charged-particle momentum resolution at 1 GeV/c is 0.5%, and resolution of the ionization energy loss in the MDC (dE/dx) is 6% for electrons from Bhabha scattering. The EMC measures photon energies with a resolution of 2.5% (5%) at 1 GeV in the barrel (end cap) region. The time resolution in the TOF barrel region is 68 ps, while that in the end cap region is 110 ps. The end cap TOF system was upgraded in 2015 using multi-gap resistive plate chamber technology, providing a time resolution of 60 ps [25]. About 13% of the data (the 4.600 GeV sample) used in the current analysis predates this upgrade.

Monte Carlo (MC) simulated data samples are produced with a GEANT4-based [29] MC package, which includes the geometric description and response of the BESIII detector. The signal MC samples of $e^+e^- \rightarrow \Lambda_c^+\bar{\Lambda}_c^-$ with $\bar{\Lambda}_c^-$ decaying into ten specific tag modes (as described below and listed in Table 2) and $\Lambda_c^+ \rightarrow p\gamma'$, which are used to determine the detection efficiencies, are generated for each CM energy using the generator KKMC [30] incorporating initial-state radiation (ISR) effects and the beam energy spread. The inclusive MC samples, which consist of $\Lambda_c^+\bar{\Lambda}_c^-$ events, charmed meson $D_{(s)}^{(*)}$ pair production, ISR return to the charmonium(-like) ψ states at lower masses, and continuum processes $e^+e^- \rightarrow q\bar{q}$ ($q = u, d, s$), are generated to estimate the potential background. Decay modes as specified in the Particle Data Group (PDG) [33] are modeled with EVTGEN [31, 32], and the remaining unknown decays are modeled with LUNDCHARM [34, 35]. Final state radiation (FSR) from charged final state particles is incorporated using PHOTOS [36].

III. METHODOLOGY

A DT approach [22] is implemented to search for $\Lambda_c^+ \rightarrow p\gamma'$. A data sample of $\bar{\Lambda}_c^-$ baryon, referred to as the single-tag (ST) sample, is reconstructed with ten exclusive hadronic decay modes, as listed in Table 2. The subset of those events in which a signal decay $\Lambda_c^+ \rightarrow p\gamma'$ candidate is reconstructed in the system recoiling against the $\bar{\Lambda}_c^-$ candidate are denoted as DT candidates. The Λ_c^+ decay BF is determined as

$$\mathcal{B}(\Lambda_c^+ \rightarrow p\gamma') = \frac{N_{\text{obs}} - N_{\text{bkg}}}{\sum_{ij} N_{ij}^{\text{ST}} \cdot (\epsilon_{ij}^{\text{DT}} / \epsilon_{ij}^{\text{ST}})}, \quad (1)$$

where the N_{obs} is the number of observed events in the signal region from data, and N_{bkg} is the number of estimated background as explained explicitly in Section VI. The subscripts i and j represent the ST modes and the data samples at different CM energies, respectively. The parameters N_{ij}^{ST} , $\epsilon_{ij}^{\text{ST}}$ and $\epsilon_{ij}^{\text{DT}}$ are the ST yields, ST and DT detection efficiencies, respectively.

IV. ST EVENT SELECTIONS

Charged tracks detected in the MDC are required to be within a polar angle (θ) range of $|\cos \theta| < 0.93$, where θ is defined with respect to the positron beam direction. For prompt tracks not from K_S^0 and $\bar{\Lambda}$ decays, the distances of the closest approach to the interaction point (IP) are required to be within ± 10 cm along the beam direction and 1 cm in the plane perpendicular to the beam (referred to as tight track hereafter). The particle identification (PID) is implemented by combining measurements of the dE/dx and the flight time in the TOF. Every charged track is assigned a particle type of pion, kaon or proton, by choosing the type with the highest probability.

Photon candidates are selected from showers reconstructed in the EMC. The deposited energy of each shower must be more than 25 MeV in the barrel region ($|\cos \theta| \leq 0.80$) or more than 50 MeV in the end cap region ($0.86 \leq |\cos \theta| \leq 0.92$). To suppress electronic noise and showers unrelated to the event, the difference between the EMC time and the event start time is required to be within (0, 700) ns. The π^0 candidates are reconstructed from photon pairs with an invariant mass in the range (0.115, 0.150) GeV/c^2 . To improve the resolution, a kinematic fit is performed constraining the invariant mass of the photon pair to the known π^0 mass [33]. The corresponding χ^2 of the fit must be less than 200. The momenta updated by the kinematic fit are used in further analysis.

Candidates for K_S^0 and $\bar{\Lambda}$ are reconstructed in their decays to $\pi^+\pi^-$ and $\bar{p}\pi^+$, respectively. Each charged track must have a distance of closest approach to the IP within ± 20 cm along the beam direction (referred to as loose track hereafter). To improve the signal purity,

PID is applied to the proton candidates, but not the pion candidates. A secondary vertex fit is performed to each K_S^0 or $\bar{\Lambda}$ candidate, and the momenta updated by the fit are used in the further analysis. To keep a high signal efficiency, a K_S^0 or $\bar{\Lambda}$ candidate is accepted if the χ^2 of this fit is less than 100. Furthermore, the decay vertex is required to be separated from the IP by a distance of at least twice the fitted vertex resolution, and the invariant mass must be within (0.487, 0.511) GeV/c^2 for $\pi^+\pi^-$ or (1.111, 1.121) GeV/c^2 for $\bar{p}\pi^+$. The $\bar{\Sigma}^0$ and $\bar{\Sigma}^-$ candidates are reconstructed with the $\gamma\bar{\Lambda}$ and $\bar{p}\pi^0$ final states, requiring the invariant masses to lie within (1.179, 1.203) GeV/c^2 and (1.176, 1.200) GeV/c^2 , respectively.

The ST $\bar{\Lambda}_c^-$ candidates are identified using the beam constrained invariant mass $M_{\text{BC}} = \sqrt{E_{\text{beam}}^2/c^4 - |\vec{p}_{\bar{\Lambda}_c^-}|^2/c^2}$ and energy difference $\Delta E = E_{\bar{\Lambda}_c^-} - E_{\text{beam}}$, where E_{beam} is the beam energy, $E_{\bar{\Lambda}_c^-}$ and $\vec{p}_{\bar{\Lambda}_c^-}$ are the energy and momentum of the $\bar{\Lambda}_c^-$ candidate in the e^+e^- CM frame, respectively. The $\bar{\Lambda}_c^-$ candidates are required to satisfy the tag-mode dependent ΔE requirements, the asymmetric intervals of which take into account the effects of ISR and correspond to three times the resolution around the peak, as summarized in Table 2. If there are more than one candidate satisfying the above requirements for a specific tag mode, the one with the minimum $|\Delta E|$ is kept.

Table 2: ΔE requirement, the ST yield, and the ST detection efficiency of each tag mode for data sample at $\sqrt{s} = 4.600$ GeV. The uncertainty in the ST yield is statistical only.

	ΔE (MeV)	N_i^{ST}	$\epsilon_i^{\text{ST}}(\%)$
$\bar{p}K^+\pi^-$	(-34, 20)	6705 ± 90	51.0
$\bar{p}K_S^0$	(-20, 20)	1268 ± 37	56.2
$\Lambda\pi^-$	(-20, 20)	741 ± 28	47.7
$\bar{p}K^+\pi^-\pi^0$	(-30, 20)	1539 ± 57	15.4
$\bar{p}K_S^0\pi^0$	(-30, 20)	485 ± 29	18.4
$\Lambda\pi^-\pi^0$	(-30, 20)	1382 ± 49	16.6
$\bar{p}K_S^0\pi^+\pi^-$	(-20, 20)	512 ± 29	19.9
$\bar{\Lambda}\pi^+\pi^-$	(-20, 20)	646 ± 31	13.7
$\bar{\Sigma}^0\pi^-$	(-20, 20)	404 ± 22	22.5
$\bar{\Sigma}^-\pi^+\pi^-$	(-30, 20)	872 ± 38	18.1

For the $\bar{\Lambda}_c^- \rightarrow \bar{p}K_S^0\pi^0$ ST mode, candidate events with $M_{\bar{p}\pi^+} \in (1.100, 1.125)$ GeV/c^2 and $M_{\bar{p}\pi^0} \in (1.170, 1.200)$ GeV/c^2 are vetoed to avoid double counting with the $\bar{\Lambda}_c^- \rightarrow \bar{\Lambda}\pi^-\pi^0$ or $\bar{\Lambda}_c^- \rightarrow \bar{\Sigma}^-\pi^+\pi^-$ ST modes, respectively. For the $\bar{\Lambda}_c^- \rightarrow \bar{\Sigma}^-\pi^+\pi^-$ ST mode, candidate events with $M_{\pi^+\pi^-} \in (0.490, 0.510)$ GeV/c^2 and $M_{\bar{p}\pi^+} \in (1.110, 1.120)$ GeV/c^2 are rejected to avoid double counting with the $\bar{\Lambda}_c^- \rightarrow \bar{p}K_S^0\pi^0$ or $\bar{\Lambda}_c^- \rightarrow \bar{\Lambda}\pi^-\pi^0$ ST modes, respectively. In the $\bar{\Lambda}_c^- \rightarrow \bar{p}K_S^0\pi^+\pi^-$ and $\bar{\Lambda}\pi^-\pi^+\pi^-$ selections, candidate events with $M_{\bar{p}\pi^+} \in (1.100, 1.125)$ GeV/c^2 and $M_{\pi^+\pi^-} \in (0.490, 0.510)$ GeV/c^2 are rejected, respectively.

The M_{BC} distributions of candidates for the ten ST

modes with the data sample at $\sqrt{s} = 4.600$ GeV are illustrated in Fig. 2, where clear $\bar{\Lambda}_c^-$ signals are observed in each mode. No peaking background is found using the inclusive MC samples. To obtain the ST yields, unbinned maximum likelihood fits on these M_{BC} distributions are performed, where the signal shape is modeled with the MC-simulated shape convolved with a Gaussian function representing for the resolution difference between data and MC simulation, and the background shape is described by the ARGUS function [37]. The candidates with $M_{BC} \in (2.275, 2.310)$ GeV/c^2 are retained for further analysis, and the signal yields for the individual ST modes are summarized in Table 2. The same procedure is performed for the other six data samples at different CM energies, the results can be found in Ref. [38] and its supplemental material. The sum of ST yields for all data samples at different CM energies is 105244 ± 384 , where the uncertainty is statistical.

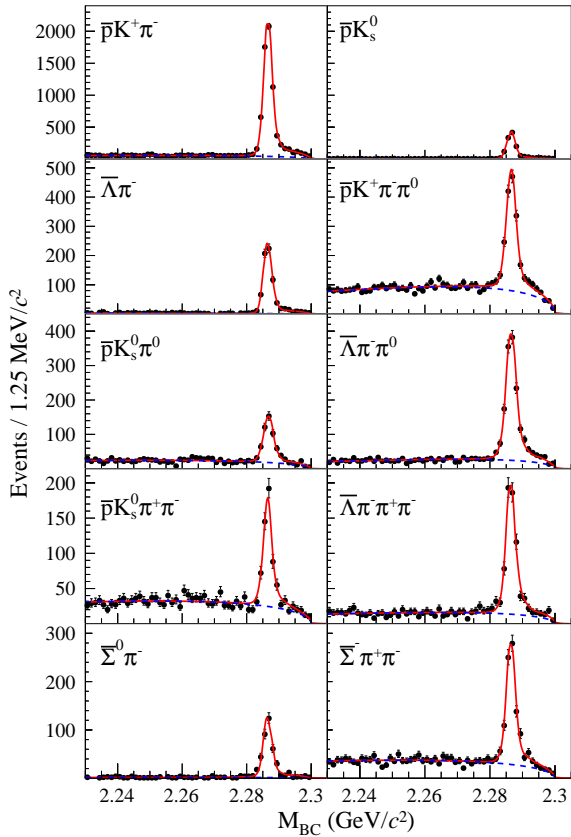


Fig. 2: The M_{BC} distributions of the ST modes for data sample at $\sqrt{s} = 4.600$ GeV. The points with error bars represent data. The red solid curves indicate the fit results and the blue dashed curves describe the background shapes.

V. RECONSTRUCTION OF $p\gamma'$ CANDIDATES

The decay $\Lambda_c^+ \rightarrow p\gamma'$ is searched for among the remaining tracks and showers recoiling against the $\bar{\Lambda}_c^-$ candidates. Only one tight track is allowed, and it must satisfy the PID criteria $\mathcal{L}(p) > \mathcal{L}(K)$ and $\mathcal{L}(p) > \mathcal{L}(\pi)$. To suppress contamination from long-lifetime particles in the final state, the candidate events are further required to be without any unused loose tracks. The γ' does not interact directly with SM fermions and thus it deposits no energy in the EMC. Backgrounds containing a π^0 are vetoed with the requirement of $E_{\max} < 0.3$ GeV and $E_{\sum} < 0.5$ GeV, where E_{\max} and E_{\sum} are the maximum energy and the energy sum of the unused showers, respectively. The γ' signal is selected using the square of the recoil mass, $M_{\text{rec}(\bar{\Lambda}_c^- p)}^2$, against the ST $\bar{\Lambda}_c^-$ and p .

After imposing all selection conditions mentioned above, the distribution of $M_{\text{rec}(\bar{\Lambda}_c^- p)}^2$ of the accepted DT candidate events from the combined seven data samples at different CM energies is shown in Fig. 3(a). There is a peaking structure at the K_L^0 mass position, from the process $\Lambda_c^+ \rightarrow p K_L^0$.

VI. BACKGROUND ANALYSIS

The potential background can be classified into two categories: those directly originated from continuum hadron production in the e^+e^- annihilation, denoted as $q\bar{q}$ background, and those from the $e^+e^- \rightarrow \Lambda_c^+\bar{\Lambda}_c^-$ events, denoted as $\Lambda_c^+\bar{\Lambda}_c^-$ background. The distribution and magnitude of $\Lambda_c^+\bar{\Lambda}_c^-$ background are estimated with the inclusive MC samples, where the peaking background $\Lambda_c^+ \rightarrow p K_L^0$ is extracted separately from the inclusive MC samples. The $\Lambda_c^+ \rightarrow p K_L^0$ rate is normalized to the known BF [33] and the remaining backgrounds are normalized to $\Lambda_c^+\bar{\Lambda}_c^-$ data yields. The $q\bar{q}$ background is investigated with M_{BC} sideband region (2.21, 2.26) GeV/c^2 of ST candidates in data, which is then reweighted to agree with those of the data in signal region. The $q\bar{q}$ and $\Lambda_c^+\bar{\Lambda}_c^-$ backgrounds are estimated to be 7.4 ± 0.4 and 7.2 ± 1.4 , respectively. The resultant $M_{\text{rec}(\bar{\Lambda}_c^- p)}^2$ distribution is depicted in Fig. 3(a).

VII. UPPER LIMIT SETTING

In order to extract the signal yield, a signal region is defined as $(0.0, 0.1) \text{ GeV}^2/c^4$ in the $M_{\text{rec}(\bar{\Lambda}_c^- p)}^2$ distribution, corresponding to a 96% signal detection efficiency after imposing all the selection criteria. The distribution of $M_{\text{rec}(\bar{\Lambda}_c^- p)}^2$ in the signal region is shown in Fig. 3(b). Thirteen candidate events are observed in the signal region, while the background events are estimated to be 14.6 ± 1.5 , where the uncertainty is statistical only. The Λ_c^+ decay BF is determined as in Eq. (1). The detec-

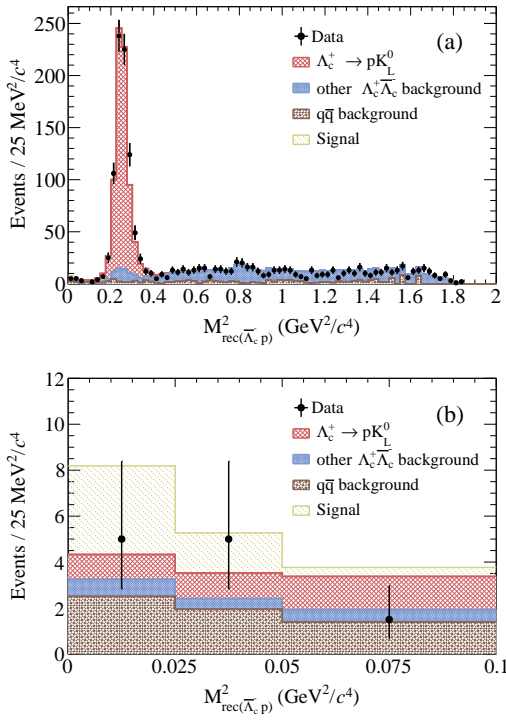


Fig. 3: (a) The full spectrum of $M^2_{\text{rec}(\bar{\Lambda}_c^- p)}$ of the accepted DT candidate events from the combined seven data samples. (b) The spectrum of $M^2_{\text{rec}(\bar{\Lambda}_c^- p)}$ of the accepted DT candidate events from the combined data in the signal region. The black points with error bars are data; no events have been observed in the last bin. The red hatched histogram indicates pK_L^0 background. The blue hatched histogram is the $\Lambda_c^+\bar{\Lambda}_c^-$ background excluding $\Lambda_c^+ \rightarrow pK_L^0$ process. The brown hatched histogram represents the $q\bar{q}$ background. The yellow hatched histogram is the $\Lambda_c^+ \rightarrow p\gamma'$ signal, which is normalized to data luminosity with the upper limit of the BF.

tion efficiency $\epsilon_{ij}^{\text{ST}}$ is obtained with the same procedure as in Ref. [38], and the $\epsilon_{ij}^{\text{DT}}$ is derived with the signal MC samples. The DT efficiencies are summarized in Table 3.

Table 3: The DT detection efficiencies in percentage for ten tag modes and seven data samples at different CM energies. The statistical uncertainties are lower than 0.3%.

\sqrt{s} (GeV)	4.600	4.612	4.628	4.641	4.661	4.682	4.699
$\bar{p}K^+\pi^-$	34.3	33.8	32.3	32.0	31.6	31.3	30.7
$\bar{p}K_S^0$	39.1	37.1	34.6	33.6	33.9	32.8	31.8
$\bar{\Lambda}\pi^-$	32.9	30.5	29.1	29.5	28.5	26.9	25.4
$\bar{p}K^+\pi^-\pi^0$	12.9	12.4	12.3	12.6	11.9	11.9	11.5
$\bar{p}K_S^0\pi^0$	14.9	14.2	13.5	13.4	13.4	13.5	12.7
$\bar{\Lambda}\pi^-\pi^0$	13.6	12.7	12.2	12.3	12.0	11.6	11.2
$\bar{p}K_S^0\pi^+\pi^-$	15.4	14.5	13.7	13.6	13.4	13.3	13.2
$\bar{\Lambda}\pi^-\pi^+\pi^-$	10.4	9.8	9.3	9.6	9.3	9.3	9.1
$\bar{\Sigma}^0\pi^-$	18.8	17.7	17.1	16.2	14.7	14.6	15.0
$\bar{\Sigma}^-\pi^+\pi^-$	17.5	16.5	16.3	16.2	15.8	15.0	14.9

Since no significant signal is observed, the profile-likelihood approach [39] is used to determine the upper limit on the BF of $\Lambda_c^+ \rightarrow p\gamma'$. The likelihood function which depends on the parameter of interest $\mathcal{B}(\Lambda_c^+ \rightarrow p\gamma')$ and the nuisance parameters $\theta = (\epsilon_{\text{eff}}, N_{\text{bkg}})$ is defined as:

$$\mathcal{L}(\mathcal{B}(\Lambda_c^+ \rightarrow p\gamma'), \theta) = P(N_{\text{obs}}|N_{\text{exp}}) \cdot G(\theta) \quad (2)$$

where the observed events are assumed to follow a Poisson distribution (P). The N_{exp} is the expected number of events; it is defined as the sum of the number of background events and number of signal events estimated in the signal region, corresponding to Eq. (1). The detection efficiency ϵ_{eff} and N_{bkg} follow Gaussian distributions (G). The upper limit on the BF of $\Lambda_c^+ \rightarrow p\gamma'$ is determined by scanning the parameter of interest. The resultant profile-likelihood scan distribution is presented in Fig. 4. The upper limit is calculated to be $\mathcal{B}(\Lambda_c^+ \rightarrow p\gamma') < 8.0 \times 10^{-5}$ at 90% confidence level (CL), where the statistical and systematic uncertainties are all incorporated. The systematic uncertainties associated with the detection efficiency and the background estimation are performed with the two nuisance parameters in a profile-likelihood fit.

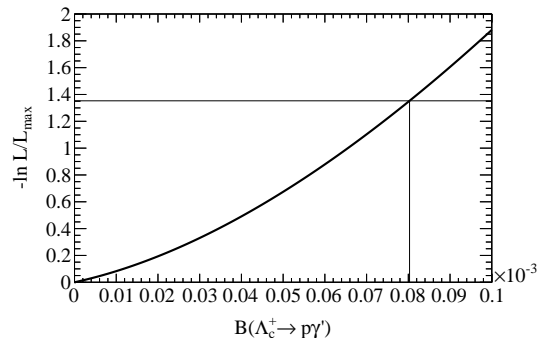


Fig. 4: The profile-likelihood curve versus $\mathcal{B}(\Lambda_c^+ \rightarrow p\gamma')$. The black solid curve is the scan result with systematic uncertainties. The cross of the curve indicates the upper limit of the BF at 90% CL.

VIII. SYSTEMATIC UNCERTAINTY

The systematic uncertainties for the BF measurement include those associated with the ST yields (N_{ij}^{ST}), reconstruction efficiencies of the ST $\bar{\Lambda}_c^-$ ($\epsilon_{ij}^{\text{ST}}$) and reconstruction efficiencies of the DT ($\epsilon_{ij}^{\text{DT}}$). As the DT technique is adopted, the systematic uncertainties originating from reconstructing the ST side largely cancel. Table 4 summarizes the possible sources of systematic uncertainties. Each of them is evaluated relative to the measured BF. The details are described below.

The uncertainties associated with the proton tracking and PID efficiencies are determined with the control sample $J/\psi \rightarrow p\bar{p}\pi^+\pi^-$ [40]. The systematic uncertainties in proton tracking and PID are assigned to be 1.0% each.

The uncertainty in the ST yields is 0.5%, which arises from the statistical uncertainty and fitting M_{BC} distributions. The uncertainty in the fitting procedure is evaluated by varying the ARGUS background parameter and changing the Gaussian function to a sum of two Gaussian functions.

The systematic uncertainty for the requirements of E_{\max} and E_{sum} is studied using the control sample of $\Lambda_c^+ \rightarrow pK^-\pi^+$. The systematic uncertainty, 3.0%, is determined by comparing the efficiencies between data and MC simulation.

According to Eq. (1), the uncertainty related to the ST efficiency is expected to be canceled. However, due to the different multiplicities of tracks and showers in the rest of the event, the ST efficiencies estimated with the generic and the signal MC samples are expected to differ slightly. Thus, the uncertainty associated with the ST efficiency is not canceled fully, which results in a so called “tag bias” uncertainty. The difference of ST efficiency between generic and the signal MC samples, 0.9%, is assigned as the corresponding uncertainty.

The uncertainty in the $q\bar{q}$ background estimation is obtained by widening the M_{BC} sideband range by 5 MeV/ c^2 in comparison to the nominal one, yielding 4.1%. In addition, the statistical uncertainty of 5.7% on the data yield in the M_{BC} sideband range (2.21, 2.26) GeV/ c^2 is taken into account. The total $q\bar{q}$ background systematic uncertainty of 7.0% is the quadratic sum of these two effects.

The main $\Lambda_c^+\bar{\Lambda}_c^-$ background is the $\Lambda_c^+ \rightarrow pK_L^0$ process. The uncertainty of its BF quoted from the PDG on $\mathcal{B}(\Lambda_c^+ \rightarrow pK_S^0)$ [33] is 5.0%, and the fraction of pK_L^0 in the signal region is 36%. The net systematic uncertainty in $\Lambda_c^+\bar{\Lambda}_c^-$ background estimation is thus 1.8%.

Other uncertainties are negligible. Assuming that all the sources of the uncertainties are uncorrelated, the total systematic uncertainties associated with the detection efficiency and the background estimation are 3.5% and 7.2%, respectively.

Table 4: The systematic uncertainties in percentage for $\Lambda_c^+ \rightarrow p\gamma'$.

mode	uncertainty (%)
p tracking	1.0
p PID	1.0
ST yield	0.5
E_{\max} and E_{sum} requirements	3.0
Tag bias	0.9
$q\bar{q}$ background estimation	7.0
$\Lambda_c^+\bar{\Lambda}_c^-$ background estimation	1.8

IX. SUMMARY

In summary, with a sample of 4.5 fb^{-1} collected at CM energies between 4.600 and 4.699 GeV with the BESIII detector, the first investigation for a massless dark photon in $\Lambda_c^+ \rightarrow p\gamma'$ decay is carried out. No significant signal is observed with respect to the expected background. The upper limit on the BF of $\Lambda_c^+ \rightarrow p\gamma'$ is measured to be $\mathcal{B}(\Lambda_c^+ \rightarrow p\gamma') < 8.0 \times 10^{-5}$ at 90% CL. It is below the sensitivity of theory prediction in Ref. [21], which predicts the BF to be 1.6×10^{-5} or 9.1×10^{-6} with different inputs of form factors. A more stringent constrain on $\mathcal{B}(\Lambda_c^+ \rightarrow p\gamma')$ is expected in the near future with larger Λ_c^+ samples at BESIII [24].

ACKNOWLEDGEMENTS

The BESIII collaboration thanks the staff of BEPCII, the IHEP computing center and the supercomputing center of the University of Science and Technology of China (USTC) for their strong support. Authors are grateful to Jusak Tandean for enlightening discussions. This work is supported in part by National Key R&D Program of China under Contracts Nos. 2020YFA0406400, 2020YFA0406300; National Natural Science Foundation of China (NSFC) under Contracts No. 11635010, No. 11735014, No. 11835012, No. 11935015, No. 11935016, No. 11935018, No. 11961141012, No. 12022510, No. 12025502, No. 12035009, No. 12035013, No. 12192260, No. 12192261, No. 12192262, No. 12192263, No. 12192264, No. 12192265, No. 12005311; the Fundamental Research Funds for the Central Universities, Sun Yat-sen University, University of Science and Technology of China; 100 Talents Program of Sun Yat-sen University; the Chinese Academy of Sciences (CAS) Large-Scale Scientific Facility Program; Joint Large-Scale Scientific Facility Funds of the NSFC and CAS under Contract No. U1832207; 100 Talents Program of CAS; The Institute of Nuclear and Particle Physics (INPAC) and Shanghai Key Laboratory for Particle Physics and Cosmology; ERC under Contract No. 758462; European Union’s Horizon 2020 research and innovation programme under Marie Skłodowska-Curie grant agreement under Contract No. 894790; German Research Foundation DFG under Contracts Nos. 443159800, Collaborative Research Center CRC 1044, GRK 2149; Istituto Nazionale di Fisica Nucleare, Italy; Ministry of Development of Turkey under Contract No. DPT2006K-120470; National Science and Technology fund; National Science Research and Innovation Fund (NSRF) via the Program Management Unit for Human Resources & Institutional Development, Research and Innovation under Contract No. B16F640076; STFC (United Kingdom); Suranaree University of Technology (SUT), Thailand Science Research and Innovation (TSRI), and National Science Research and Innovation Fund (NSRF) under Contract No. 160355; The Royal Society, UK under Contracts Nos. DH140054, DH160214;

The Swedish Research Council; U. S. Department of Energy under Contract No. DE-FG02-05ER41374.

-
- [1] S. L. Glashow, J. Iliopoulos, and L. Maiani, Phys. Rev. D **2**, 1285, (1970).
- [2] M. Tanabashi *et al.* (Particle Data Group), Phys. Rev. D **98**, 030001 (2018).
- [3] C. S. Aulakh and R. N. Mohapatra, Phys. Lett. B **119**, 136 (1982).
- [4] S. Glashow and S. Weinberg, Phys. Rev. D **15**, 1958 (1977).
- [5] B. Holdom, Phys. Lett. B **166**, 196 (1986).
- [6] B. A. Dobrescu, Phys. Rev. Lett. **94**, 151802 (2005).
- [7] E. Gabrielli, B. Mele, M. Raidal, and E. Venturini, Phys. Rev. D **94**, 115013 (2016).
- [8] M. Fabbrichesi, E. Gabrielli, and B. Mele, Phys. Rev. Lett. **119**, 031801 (2017).
- [9] J. Y. Su and J. Tandean, Phys. Rev. D **101**, 035044 (2020).
- [10] L. Ackerman, M. R. Buckley, S. M. Carroll, and M. Kamionkowski, Phys. Rev. D **79**, 023519 (2009).
- [11] J. X. Pan, M. He, X. G. He, and G. Li, Nucl. Phys. B **953**, 114968 (2020).
- [12] V. Barger, C. W. Chiang, W. Y. Keung, and D. Marfatia, Phys. Rev. Lett. **108**, 081802 (2012).
- [13] C. W. Chiang and P. Y. Tseng, Phys. Lett. B **767**, 289 (2017).
- [14] J. R. Batley *et al.* (NA48/2 Collaboration), Phys. Lett. B **746**, 178 (2015).
- [15] M. Pospelov, Phys. Rev. D **80**, 095002 (2009).
- [16] R. Aaij *et al.* (LHCb Collaboration), Nat. Phys. **18**, 277 (2022).
- [17] M. Ablikim *et al.* (BESIII Collaboration), Phys. Rev. D **87**, 012009 (2013).
- [18] M. Ablikim *et al.* (BESIII Collaboration), Phys. Rev. D **101**, 032001 (2018).
- [19] M. Ablikim *et al.* (BESIII Collaboration), Phys. Rev. D **105**, L071101 (2022).
- [20] M. Ablikim *et al.* (BESIII Collaboration), Phys. Rev. D **101**, 112005 (2020).
- [21] J. Y. Su and J. Tandean, Phys. Rev. D **102**, 115029 (2020).
- [22] J. Adler *et al.*, Phys. Rev. Lett. **62**, 1821 (1989).
- [23] M. Ablikim *et al.* (BESIII Collaboration), Nucl. Instrum. Meth. A **614**, 345 (2010).
- [24] M. Ablikim *et al.* (BESIII Collaboration), Chin. Phys. C **44**, 040001 (2020).
- [25] X. Li *et al.*, Radiat. Detect. Technol. Methods **1**, 13 (2017); Y. X. Guo *et al.*, Radiat. Detect. Technol. Methods **1**, 15 (2017).
- [26] M. Ablikim *et al.* (BESIII Collaboration), Chin. Phys. C **40**, 063001 (2016).
- [27] M. Ablikim *et al.* (BESIII Collaboration), arXiv:2203.03133.
- [28] M. Ablikim *et al.* (BESIII Collaboration), arXiv:2205.04809.
- [29] S. Agostinelli *et al.*, Nucl. Instrum. Meth. A **506**, 250 (2003).
- [30] S. Jadach *et al.*, Phys. Rev. D **63**, 113009 (2001).
- [31] D. J. Lange, Nucl. Instrum. Meth. A **462**, 152 (2001).
- [32] R. G. Ping, Chin. Phys. C **32**, 599 (2008).
- [33] P. A. Zyla *et al.* (Particle Data Group), Prog. Theor. Exp. Phys. **2020**, 083C01 (2020) and 2021 update.
- [34] J. C. Chen, G. S. Huang, X. R. Qi, D. H. Zhang, and Y. S. Zhu, Phys. Rev. D **62**, 034003 (2000).
- [35] R. L. Yang, R. G. Ping, H. Chen, Chin. Phys. Lett. **31**, 061301 (2014).
- [36] R. W. Elzbieta, Phys. Lett. B **303**, 163 (1993).
- [37] H. Albrecht *et al.*, Phys. Lett. B **241**, 278 (1990).
- [38] M. Ablikim *et al.* (BESIII Collaboration), Phys. Rev. Lett. **128**, 142001 (2022).
- [39] G. Cowan, K. Cranmer, E. Gross and O. Vitells, Eur. Phys. J. C **71**, 1554 (2011).
- [40] M. Ablikim *et al.* (BESIII Collaboration), Chin. Phys. C **40**, 026201 (2016).